EVIDENCE OF COUNTER-DIFFERENCE SURFACE HEAT FLUXES AND ITS HYPOTHESES

Edi Santoso[1]

Abstract

Parameterization of surface heat flux estimates near-surface turbulent heat fluxes from differences of potential temperature between the surface skin and the mid-mixed layer (ML). The rate of this turbulent transport is proportional to the product of a convective velocity times an empirical transport coefficient. New data from three different sites within Boundary Layer Experiment - 1996 (BLX96) are used to evaluate surface heat flux parameterization. Old data from six other field programs (BLX83, Koorin, FIFE, Monsoon 90, HAPEX-MOBILHY, and TOGA-COARE) are re-analyzed to test this parameterization. Evidence from virtually all of these experiments indicates that the empirical transport coefficient for heat fluxes (C_{*H}) does not depend on surface roughness. Positive turbulent heat fluxes are observed to exist near the bottom of the ML even when there is zero potential temperature difference ($\Delta\overline{q}$=0) between the surface skin and the mid-ML. Evidence suggests that positive heat fluxes could also occur when the surface skin has a slightly colder potential temperature than the mid-ML, implying a flux that is opposite or counter to the potential-temperature difference. Such counter-difference fluxes could be explained by an infrared radiative transfer from the surface skin, or by non-equilibrium conditions during rapidly-changing insolation near sunset.

Intisari

Fluks panas turbulen dekat permukaan dapat diestimasi dari selisih antara suhu potensial di batas permukaan (surface skin) dan di bagian tengah lapisan tercampur (mid-mixed layer). Kecepatan dari transpor turbulen ini sebanding dengan perkalian antara koefisien empiris transpor dengan kecepatan konvektif. Data baru dari hasil pengukuran BLX96 pada 3 lokasi yang berbeda akan digunakan untuk mengevaluasi parameterisasi ini. Sementara data yang diperoleh dari yang pernah dilakukan sebelumnya (BLX83, Koorin, FIFE, Monsoon 90, HAPEX-MOBILHY, and TOGA-COARE) digunakan untuk menguji hasil parameterisasi ini. Hasil yang diperoleh mengindikasikan bahwa koefisien empiris transpor untuk fluks panas tidak tergantung pada kekasaran permukaan (surface roughness). Bukti juga menunjukkan bahwa fluks panas positif dapat terjadi ketika suhu potensial di surface skin sama atau sedikit lebih dingin daripada di mid-mixed layer. Kejadian seperti ini, disebut counter-difference fluxes, dapat dijelaskan dengan tranfer radiasi infra merah dari surface skin atau dengan kondisi ketidaksetimbangan perubahan secara cepat insolasi saat mendekati matahari terbenam.

1. INTRODUCTION

Most of the atmospheric boundary-layer turbulence is generated buoyantly by thermals rather than mechanically by wind shear during convective conditions with calm to light winds, (Stull, 1997a). Thermal diameters are sufficiently large (order of 1 to 2 km) that the very large central core in each thermal is protected from small-eddy lateral entrainment (Crum et al., 1987). The vertical transport by thermals is a large-eddy vertical-advection-like process (Stull, 1995) with a rate of transport proportional to the Deardorff velocity. Within this core, air parcels from near the surface rise to the middle and the top of the convective boundary layer (BL) with virtually no dilution (Stull and Eloranta, 1985). Because buoyant thermals are an isotropic with greater energy in the vertical, they efficiently transport heat, momentum and moisture vertically from the surface.

Stull (1994, 1997b) utilized these characteristics of convection to show that during free convection the surface vertical turbulent flux

$\overline{w'y'}$ of any mean variable $\overline{y}$ is proportional to the Deardorff velocity times the difference of $\overline{y}$ between the surface skin and the mid-mixed layer (ML). The term ML is used to represent the whole convective BL between the surface and the top of the BL (z_i). A sub domain within the interior of the ML is called the uniform layer (UL; Santoso and Stull, 1998), because within that region wind speed and potential temperature are nearly uniform with height.

Convective transport theory (CTT) that was first suggested by Stull (1994) parameterized surface heat fluxes for convective conditions. By using surface skin and the UL values in the formulation, he proposed that surface heat flux parameterization should be independent of roughness length for free convection, a hypothesis that will be tested here. The theory was originally calibrated with data from Boundary Layer Experiment-1983 (BLX83) in Oklahoma (Stull and Eloranta, 1984), and was independently validated using data from the Koorin experiment in Australia (Clarke and Brook, 1979).

CTT and the evaluation of its empirical parameters have been tested over a variety of sites by Kustas et al. (1996), Greischar and Stull (1998), Chang & Grossman (1998), and Lundquist (1997). These sites include the Hydrologic Atmospheric Pilot Experiment - Modelisation du Bilan Hydrique (HAPEX-MOBILHY) conducted in southwestern France (Andre et al., 1986), the First ISLSCP Field Experiment (FIFE) conducted in eastern Kansas (Sellers et al. 1988), the Monsoon 90 experiment conducted in southeastern Arizona (Kustas et al., 1991), the Tropical Ocean-Global Atmosphere - Coupled Ocean-Atmosphere Response Experiment (TOGA-COARE) conducted in western Pacific (Bond and Alexander, 1994), and the 1997 Cooperative Atmospheric-Surface Exchange Study (CASES97) conducted in Kansas (LeMone et al., 1998, LeMone and Grossman, 1998).

Kustas and colleagues found that satellite-derived surface skin conditions must be used with care in a forest, because of the difference between the solar illuminated sides of the trees and the partially shaded sides that are viewed by remote sensors. Greischar and Stull, and Chang and Grossman, found CTT to work over the Pacific Ocean warm pool, but with slightly different values of the empirical parameters. Lundquist also found parameter values to vary by site (rangeland/pasture vs. winter wheat), and suggested that the parameters for scalars (potential temperature, virtual potential temperature, and mixing ratio) are not identical. Beljaars (1995) and Sorbjan (1995, 1997) argue that the CTT parameters should also depend on the surface roughness, based on the success of roughness-based surface-layer and micro-layer similarity theories.

A new BL field experiment (BLX96) was conducted in Oklahoma and Kansas over three sites with different aerodynamic roughness (Stull et al., 1997) to test the parameterization and its empirical parameter. The goal of the present paper is to test, refine, and better understand the capabilities and limitations of surface heat flux parameterization. Detailed results from BLX96 will be given along with re-analyses of six other published data sets. It will be shown that there is no dependence of the coefficients of heat flux on the surface roughness, in contrast to that of momentum flux.

2. CTT AS A SURFACE HEAT FLUX PARAMETERIZATION

CTT gives the following surface heat flux relationship (Stull, 1994):

$$\overline{w'\theta'}_s = C_{*H} \cdot w_* \cdot \Delta\overline{\theta} \qquad (1)$$

where C_{*H} is the dimensionless, empirical ML coefficient for heat, and w_* is the Deardorff velocity that is shown in the following equation:

$$w_* = \left[\left(g / T_v\right) \cdot z_i \cdot \overline{w'\theta_v'}_s\right] \qquad (2)$$

where g is gravitational acceleration, T_v is virtual absolute temperature, z_i is the convective BL depth, $\overline{w'\theta_v'}_s$ is vertical virtual temperature flux near the surface, and subscript s denotes near-surface characteristics.

The last factor in (1) is a difference between the surface skin condition and the value in the UL, for potential temperature $\Delta\overline{\theta} = \overline{\theta}_{skin} - \overline{\theta}_{UL}$.

Eq. (1) is in implicit form, because the surface heat flux on the left side is a function of surface heat and moisture fluxes hidden in w_* on the right side. This is because w_* is a function of $\overline{w'\theta_v'}_s \approx \overline{w'\theta'}_s \cdot \left(1 + 0.61 \cdot \overline{r}\right) + 0.61 \cdot \overline{\theta} \cdot \overline{w'r'}_s$, where r is mixing ratio and $\overline{w'r'}_s$ is surface moisture flux.

Fortunately, that equation is easy to manipulate into explicit form (Stull 1994), yielding:

$$\overline{w'\theta'}_s = b_H \cdot w_B \cdot \Delta\overline{\theta} \qquad (3)$$

where b_H is the dimensionless empirical convective transport coefficient for surface heat flux, and w_B is buoyancy velocity that is shown by following equation:

$$w_B = \left[\left(g / T_v\right) \cdot z_i \cdot \Delta\overline{\theta}_B\right]^{1/2} \qquad (4)$$

Stull (1994) showed theoretically and empirically to get a relationship between w_* and w_B:

$$w_* = b_H{}^{1/3} \cdot w_B \qquad (5)$$

3. RESULTS OF PREVIOUS STUDIES

In evaluating the empirical ML transport coefficient for surface heat flux, Stull (1994) used data from the BLX83 field experiment near Chickasha, in an agricultural region in Oklahoma (Stull and Eloranta, 1984). The region was generally flat with local height variations on the order of 15 m and gentle average slope toward the east with gradient 1/1000. The average aerodynamic roughness length was on the order of z_o = 0.05 m.

The result showed that the mean dimensionless ML transport coefficient and the standard deviation to be: C_{*H} = 0.0063 (± 0.0016). The associated convective transport coefficient was $b_H = C_{*H}^{3/2}$ = 0.0005 (± 0.0002). Both the CTT theory and the parameter values were found to work well when tested using independent data from the Koorin experiment (Clarke and Brook 1979) conducted in a semiarid, forested area with a grass understory in northern Australia, with average roughness of z_o = 0.4 m.

Greischar and Stull (1998) used data from the TOGA-COARE field experiment in the Western Pacific to test and validate the applicability of CTT for a tropical marine BL. The heat fluxes during this field campaign were an order of magnitude smaller than those of the BLX83 experiment. They found the dimensionless ML coefficient and the standard C_{*H} = 0.0061 (± 0.0024), and the related convective transport coefficients to be: b_H = 0.0005 (± 0.0003). While the coefficients for heat were nearly identical to those originally found at BLX83. Aerodynamic roughness length was roughly z_o =0.00003 to 0.0004 m.

Kustas et al. (1996) used data from the HAPEX – MOBILHY, FIFE, and Monsoon 90 field experiments to test CTT. The motivation was to see if satellite observations of surface skin temperature could be used to estimate surface fluxes. The forested area at the HAPEX – MOBILHY site had level topography and a relatively open canopy. The FIFE area was primarily composed of prairie grasses, with 10% coverage of trees in valley bottoms. The Monsoon 90 area was composed mostly of a grass- and shrub-dominated ecosystem. Kustas et al. (1995) applied the BLX83 transport coefficients for data from those three field experiments, and found fairly good agreement between measured and predicted fluxes for FIFE and Monsoon 90. However, predicted fluxes for HAPEX – MOBILHY were lower than the measured ones, partly because of the illumination vs. view geometries mentioned previously.

Lundquist (1997) used data from two Kansas sites obtained during the 22 April to 22 May 1997 field period of CASES97. The Beaumont site was mostly rangeland/pasture with some rolling hills and a large escarpment to the east. The Oxford site was mostly winter wheat, with patches of trees. Aerodynamic roughness in the rangeland/ pasture was roughly z_o = 0.01 m, and in the winter wheat was roughly z_o = 0.05 m. Eddy correlation fluxes were found using sonic anemometers/thermometers at 4 m height on instrumented masts, and a cross-chain loran sounding system (CLASS) was used to get mid-ML characteristics. She found C_{*H} = 0.012 (± 0.004) at Beaumont, based on 22 data points. For the Oxford site, she found C_{*H} = 0.029 (± 0.030) based on 10 data points.

All of the field programs above used the same method to find mean and standard deviation values of C_{*H}. Namely, first the C_{*H} value was found using (1) from each individual run or sub-experiment, and then the resulting set of C_{*H} values was combined to yield the reported statistics for each field program. In this research a different approach will be taken, using regression to estimate the best C_{*H} coefficients for the whole field program. This approach yields new insights into the systematic variation of coefficient values.

4. OBSERVATIONS AND ANALYSIS PROCEDURE OF BLX96 DATA

Data from the Boundary Layer Experiment – 1996 (BLX96) field experiment over Oklahoma and Kansas are used here as an additional test of CTT for heat fluxes. Relatively flat topography, large areas of uniform land use, and frequent fair weather motivated the selection of this region. The University of Wyoming King Air aircraft was flown over three different sites having different land use and surface roughness within this region, in order to determine if the empirical coefficients for heat flux are indeed independent of surface roughness. The three flight tracks were named after nearby villages: Lamont and Meeker in Oklahoma, and Winfield in Kansas, with each track length of order 70 km. A more detailed description of the goals, sites, instruments and experimental procedures of BLX96 can be found in Stull et al. (1997) and Berg et al. (1997).

The Lamont track, in Oklahoma, was primarily over crop land, and was the least rough. Terrain under the track was quite flat, but gently rising to the west, with elevations ranging from 320 to 425 m MSL (mean sea level). Vegetation coverage consisted of 60 - 80% wheat fields, 20 - 40% pasture, and a small number of trees less than 10 m tall. The average aerodynamic roughness was z_o = 0.1 m, based on direct calculations using Monin-Obukhov similarity theory for the surface layer, and using tables of roughness classifications

(Smedman-Hogstrom and Hogstrom 1978; Stull 1988; Wieringa 1980, 1986).

The Winfield track, in Kansas, was over predominantly pasture land. Small hills near the center of the track ranged from 70 to 100 m in height. Terrain was rising to the west, with elevations ranging from 250 to 400 m MSL. Vegetation coverage consisted of 30 - 60% pasture, 10 - 50% forested areas (more wooded at the east end) with trees less than 10 m tall, and the remaining area was cultivated. The average aerodynamic roughness length was z_o = 0.9 m.

The Meeker track, in Oklahoma, was over a region mainly covered by forest, and was the most rough. It had more small rolling hills that ranged from 40 to 60 m in height. Otherwise, the terrain was relatively flat, with elevations from east to west ranging from 250 to 280 m MSL. Vegetation coverage consisted of 40 - 50% pasture, 40 - 60% wooded areas with trees less than 10 m tall, and 10 - 30% cropland. The average aerodynamic roughness length was z_o = 1.4 m.

Flight patterns were designed by first "flying" a virtual aircraft along several candidate flight patterns through a hypothetical boundary layer (Santoso and Stull, 1999), and then analyzing the synthetic data collected for robustness using the criteria of Lenschow and Stankov (1986). Based on the resulting experimental design, 34 low-altitude horizontal flight legs were actually flown, each 68 to 75 km long, during 12 flights of the King Air flown between 15 July and 13 August 1996. Average heights of the low-altitude legs varied between 30 m and 75 m AGL (above ground level). Also flown at the beginning, middle, and end of the flight each day were slant ascent/descent soundings from 5 m AGL to top altitudes well above the top of the ML (top altitudes were on the order of 3 to 4 km AGL, but varied from day to day depending on the weather).

Fast rate data, sampled at 50 Hz for the three wind components, mixing ratio and temperature, were used in the eddy-correlation flux calculation for each leg. The aircraft speed was roughly 100 ms^{-1}. Sun et al.'s (1996) recommendations with slight modification were followed in calculating fluxes, considering that the low-altitude horizontal legs were flown almost following the gently-rolling surface terrain. The following criteria were used to identify the acceptable portions of the horizontal legs: aircraft pitch value of less than ± 5^o with a difference of less than 2.5^o for two any consecutive points, roll values of less than ± 10^o with a difference of less than 5^o for two any consecutive points, and no sudden changes in height (based on the two radar altimeters). In some cases there were data points in the leg that did not fulfill the above criteria. These data points were removed and replaced with missing-data flags during the post-experiment data analysis.

Before calculating fluxes, the data series were detrended, and were despiked by removing data points that were more than five standard deviations from the mean and replacing them with a linear interpolation between neighboring good data values. In order to remove the inadequately sampled mesoscale features larger than 2.5 km (equivalent to a wavelength of 5 km), Fourier analysis (Stull, 1988; Press et al., 1992) was used to filter out those wavelengths greater than 5 km. The highest frequencies (wavelengths less than 20 m) were removed, because the sensors used to measure wind, mixing ratio and temperature were mounted on different parts of the aircraft, with separation distances of up to 4 - 5 m. These filtered fluxes differed by less than 1% from the unfiltered fluxes, based on filtering experiments conducted.

The calculated kinematic heat fluxes for the low-altitude (z of order of 10 m) legs were extrapolated to the surface following Stull (1994) using $\overline{w'\theta'}_s = \overline{w'\theta'}(z) / \left[1 - 1.2 \cdot \left(z / z_i\right)\right]$. The same method was applied to calculate surface kinematic fluxes of virtual potential temperature, $\overline{w'\theta_v{}'}_s$, used later to calculate the Deardorff velocity w_*.

From vertical profiles of virtual potential temperature, mixing ratio and winds measured during the aircraft slant ascent and descent soundings, the average mixed layer depths, z_i, were estimated. Using polynomial interpolation in time to account for the nonstationarity of ML depth during the whole day's flight, z_i for each low-altitude leg at its midtime was calculated, and this z_i value was used in the calculations of w_* for that flight leg.

The next step was to calculate values of potential temperature in the UL. First, the raw slant ascent/descent sounding data were sorted into bins of 2 m height, and an average was computed for the center of each bin. An example of these bin-averaged values are plotted in Fig. 1 for 15 July 96 for temperature. There was relatively little scatter in the bin-averaged data, so we could get a robust estimate of $\overline{\theta}_{UL}$ by averaging together all the bin values between 100 m AGL to the top of the sounding (600 m AGL for this case). This height range was consistent with previous height ranges for computing the UL (Santoso and Stull, 1998). The resulting standard error of the mean was ± 0.076 K for $\overline{\theta}_{UL}$.

A downward-looking Heiman pyranometer on the aircraft was used to get surface skin temperatures (T_{skin}) averaged along the flight track. Greischar and Stull (1998) made corrections for T_{skin} due to absorption by moisture between aircraft and surface. They found that for the Western Pacific warm pool, where the mixing

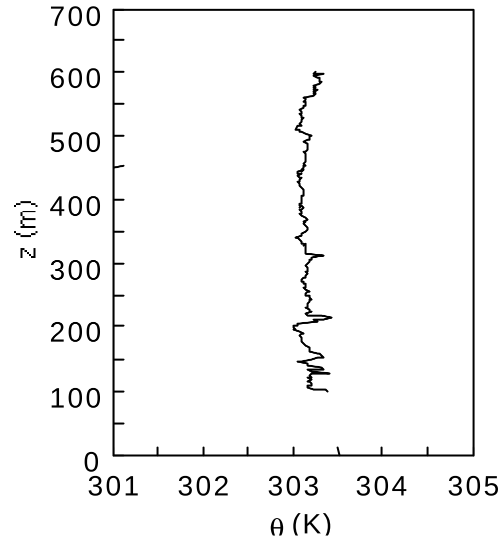

Fig. 1. Example of potential temperature profile at 1157 CDT (=UTC – 5 h) during 15 July 96, for flight leg ABA (the first of three deep soundings on this day during BLX96) showing data after averaging into 2 m vertical bins (roughly 15 data per bin). Plotted here are only the portions of the soundings that were within the uniform layer (UL).

ratio was about 18 g kg^{-1} or greater, the correction rate was linear over the lowest several hundred meters, and required a 0.06 K to 0.14 K increase in the T_{skin} estimate per 100 m increase in elevation. Perry and Moran (1994) showed from studies over semiarid rangeland that thermal IR measurements of T_{skin} made at 100 m above ground level showed little atmospheric attenuation effects, with standard deviation of temperature correction of about 0.1 K per 100 m of sensor elevation. During BLX96 the observed mixing ratios were less than 16 g kg^{-1} and near-surface flight leg heights were less than 75 m AGL, resulting in negligible (less than 0.1 K) corrections for this effect for these low-altitude legs. Finally, because the other potential temperatures in the air were defined with respect to a reference pressure of 100 kPa, T_{skin} was also converted to a potential temperature (θ_{skin}) using the same reference pressure.

There were no direct measurements of surface pressure (p_{sfc}) under the flight tracks, therefore the hypsometric equation (Holton, 1992, Stull, 1995) was used to calculate a leg-averaged value of p_{sfc} based on leg averages of p, T, r, radio-altimeter height above ground, and pressure height from the aircraft aneroid altimeter. To calculate p_{sfc} the hypsometric equation was iterated down from the leg-average aircraft altitude using 1 m intervals until reaching the average ground surface. Because this technique required T and r values along the mathematical path of iteration, two approaches were tested. One test assumed that air below the flight leg was uniform with T and r equal to their leg-averaged values, and second test assumed that they increased linearly from leg-averaged values of T and r toward T_{skin} and r_{sat} (T_{skin}) at the ground surface. These two approaches probably bracket the real atmospheric temperature profile, suggesting that the estimates of p_{sfc} probably bracket the actual value. Considering all the BLX96 data, the maximum difference between these two approaches was less than 0.26 mb. Therefore, the averaged values from both approaches were used to calculate p_{sfc}, with error estimate of less than ± 0.13 mb.

5. NEW RESULTS

To find the ML transport coefficients using (1) $\overline{w'\theta'_s}$ was linearly regressed against the product $w_* \cdot \Delta\overline{\theta}$. The slope of the resulting least-squares best fit gives the desired coefficient, C_{*H}. Plots of this regression allow us to identify other characteristics of the data set that would have been hidden if the traditional approach of finding the C_{*H} coefficient had been utilized separately for each data point using (1) and then averaging the results.

In initial analysis of BLX96 data, and re-analysis of the other data sets, the linear regression is constrained to pass through the origin. The reason is that it is expected to have zero turbulent flux whenever there is zero potential temperature difference between the surface skin and the ML. However, as will be shown later, for heat flux such a constraint is not appropriate. Thus, for heat flux a second re-analysis will be performed without this constraint.

5.1 Transport Coefficients for BLX96

Fig. 2 shows the method of estimated transport coefficient C_{*H}, using different plotting symbols for the three field sites. There is less segregation of the data by sites for heat fluxes. For this reason, heat fluxes from the three sites are grouped together as a single BLX96 data set.
The figure shows the plot of kinematic surface heat flux ($\overline{w'\theta'_s}$) vs. ($w_* \cdot \Delta\overline{\theta}$) for the whole BLX96 data set. The temperature data are not as sensitive to non-free-convection cases as were the wind data (Santoso, 2000). ML transport coefficients for heat flux for each site are: C_{*H} = 0.0058 (± 0.0020) for Lamont, C_{*H} = 0.0049 (± 0.0007) for Winfield, C_{*H} = 0.0071 (± 0.0032) for Meeker, using best-fit lines through the origin. The best ML transport coefficient based on regression

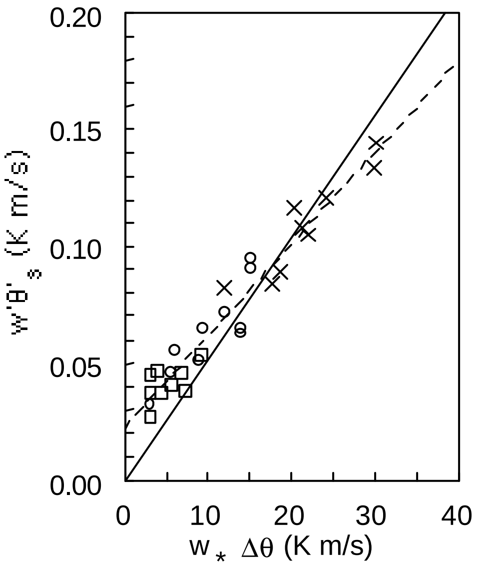

Fig. 2. Kinematic surface heat flux $\overline{w'q'_s}$ regressed against the product of Deardorff velocity w_* times potential temperature difference $\Delta\overline{q}$ between the surface skin and the uniform layer for BLX96 field experiment data [Winfield (crosses), Meeker (open squares), Lamont (open circles). One regression is forced to pass through the origin (solid line), while for the other a non-zero intercept is allowed (dashed line). In this and many subsequent figures, the overbar on the kinematic heat flux ($\overline{w'q'_s}$) is omitted in the axis labels.

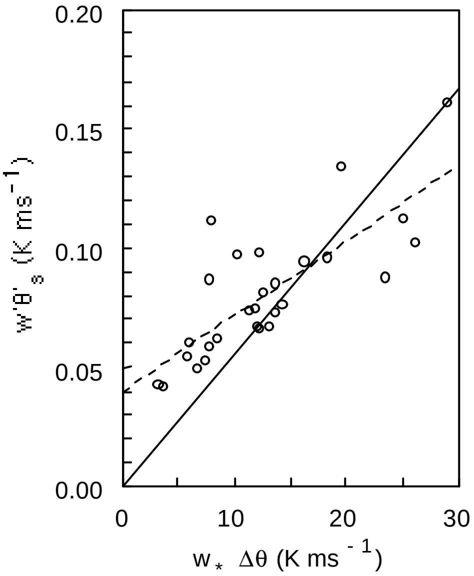

Fig. 3. Similar to Fig. 2, but for BLX83.

against the combined data from all of BLX96 is C_{*H} = 0.0052 (± 0.0029), again for a line through the origin (solid line in Fig 2).

It is obvious, however, that the best fit for heat flux is better described by a line (dashed line in Fig 2) that is not forced to pass through the origin. This issue is discussed later.

5.2. Results of Other Field Programs

To compare with CTT coefficients from other field programs, the same linear-regression approach was used to reanalyze data from BLX83, Koorin, TOGA – COARE, FIFE, Monsoon 90 and HAPEX – MOBILHY. For these analyses, the best-fit line initially is constrained to pass through the origin.

The BLX83 data were measured by instrumented aircraft over rangeland and some crops in Oklahoma. Estimated surface roughness lengths for this site were z_o = 0.05 m (Stull, 1994) based on the roughness classification tables, and z_o = 0.34 m (Beljaars, 1995) based on traditional surface-layer flux-profile relationships. Typical flight leg lengths were about 20 km, which are too short for statistically-robust statistics according to the criteria of Lenschow and Stankov (1986).

Fig. 3 shows the plots of kinematic surface heat flux ($\overline{w'q'_s}$) vs. ($w_* \cdot \Delta\overline{q}$) for all BLX83 data, where the fluxes were found using the eddy-correlation method. The new ML transport coefficient for heat flux is C_{*H} = 0.0056 (± 0.0030). The plot of the heat flux data in Fig. 3 are quite scattered because of the short flight legs.

In the Koorin experiment, the ABL and UL data were measured by radiosondings in northeast Australia over a sparse forest. Estimated surface roughness lengths were z_o = 0.4 m at site 1 and z_o = 0.9 m at site 2 (Clarke and Brook, 1979). The data analyzed for this paper were mainly from observations at site 1. Fluxes were calculated by tower-based eddy correlation. Surface skin temperatures were based on a near surface "black ball" radiometric approach (Clarke and Brook, 1979; Stull, 1994). Fig. 4 shows the new regression for the Koorin data. The new ML coefficient is C_{*H} = 0.0057 (± 0.0059). Again, the C_{*H} result is not sensitive to non-free-convection cases.

Instrumented aircraft measured TOGA – COARE data over the western tropical Pacific Ocean. The estimated surface roughness length was z_o = 0.0004 m based on surface-layer flux-profile relationships, which was within the range of values found from roughness classification tables. Typical flight legs were longer than 60 km. Possible effects of ocean currents causing nonzero wind at the surface were neglected, based on the discussion of Greischar and Stull (1998). Fig. 5 shows the regression kinematic surface heat flux ($\overline{w'q'_s}$) vs. ($w_* \cdot \Delta\overline{q}$). The new ML coefficient for heat flux is C_{*H} = 0.0073 (± 0.0021). All data on the plot are slightly scattered, but fall close to the regression line.

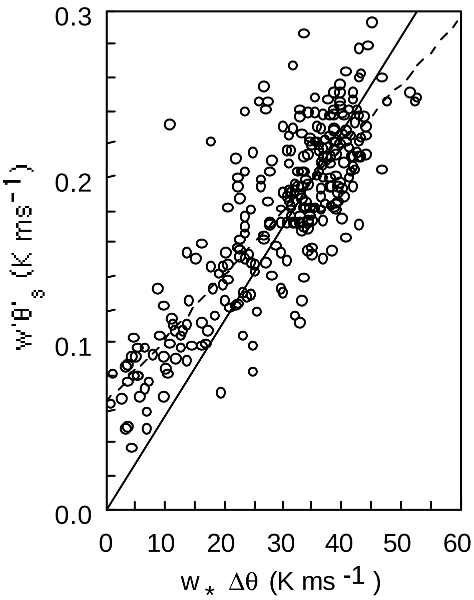

Fig. 4. Similar to Fig. 2, but for Koorin.

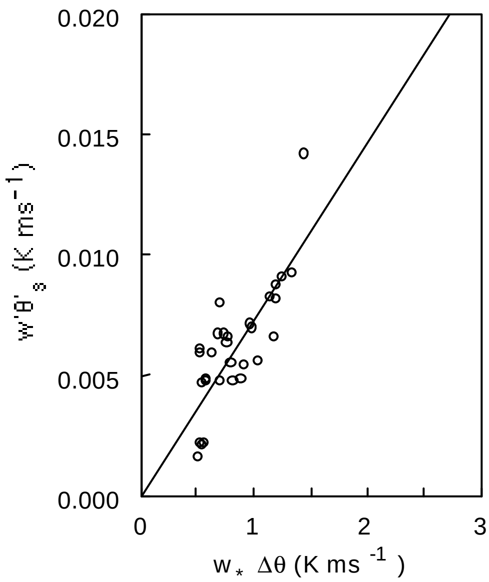

Fig. 5. Similar to Fig. 2, but for TOGA - COARE

Heat flux data from FIFE, Monsoon 90 and HAPEX - MOBILHY are presented by Kustas et al. (1996). For the FIFE experiment in Kansas over pasture and crops, the ABL and UL data were measured from radiosondings. Bet and Beljaars (see Kustas et al., 1996) estimated a surface roughness length for FIFE site of z_o = 0.19 m, while Brutsaert and Sugita (1992) found z_o = 1.05 m. Surface fluxes were estimated using tower-based temperature measurements, analyzed using the Bowen ratio method. Surface skin temperatures were derived from NOAA-9 and NOAA-11 AVHRR satellites.

In the Monsoon experiment over the Arizona dessert, the ABL and UL data were derived from radiosondings. Stewart et al. (1994) calculated that the range of roughness lengths for the site was z_o = 0.01 m to 0.03 m. Kustas et al. (1996) estimated a roughness length of z_o = 0.1 m for the site. Tower-based eddy correlation was used to calculate surface fluxes. Surface skin temperatures were determined from a ground-based network of IR thermometers. The subset of HAPEX – MOBILHY data presented by Kustas was collected by instrumented aircraft over forest and crops of southwest France. Estimated surface roughness lengths for this site were z_o = 1.2 m (Brutsaert et al., 1993) and z_o = 1.5 m (Mahrt and Ek, 1993).

The FIFE and Monsoon 90 data are plotted in Fig. 6. The best-fit coefficients are C_{*H} = 0.0055 (± 0.0024) for FIFE, and C_{*H} = 0.0050 (± 0.0045) for Monsoon 90 (regression lines not shown in Fig. 6). These coefficients plus/minus their standard deviations overlap significantly, as might be expected by the relatively close clustering of the original data apparent in Fig 6. If treated as a single unified data set, the new ML coefficient for heat flux is C_{*H} = 0.0051 (± 0.0040), for the solid line in Fig 6.

The HAPEX data plotted in Fig. 7 give C_{*H} = 0.012 (± 0.002). Again in these experiments, all data are distributed quite well around regression lines.

The C_{*H} values show no significant correlation with z_o, as shown in Fig. 8. Good agreement is found for heat-flux ML coefficients over land sites, except for HAPEX - MOBILHY data that is about twice as large as the others. The coefficient over water is slightly larger than those over land. For the subset of data that were measured from aircraft platforms (BLX96, BLX83 and HAPEX - MOBILHY), the data plots are less scattered and the standard deviations of the heat flux coefficients are smaller. Because of other effects on C_{*H} that are discussed in next subsection, calculating an overall average value of C_{*H} is postponed.

Heat flux data from virtually all the sites studied here suggests that there can be a positive turbulent heat flux even with no potential temperature difference $\Delta\bar{q}$. This is explored next.

5.3. *Non-zero intercept in Heat Flux Plots*

In the plots of heat flux $(\overline{w'q'_s})$ vs. $(w_* \cdot \Delta\bar{q})$ of Figs. 2 – 7, the data exhibit a noticeably different slope and intercept than the regressed lines forced through the origin. Using a different way of plotting the TOGA-COARE data, Grant and

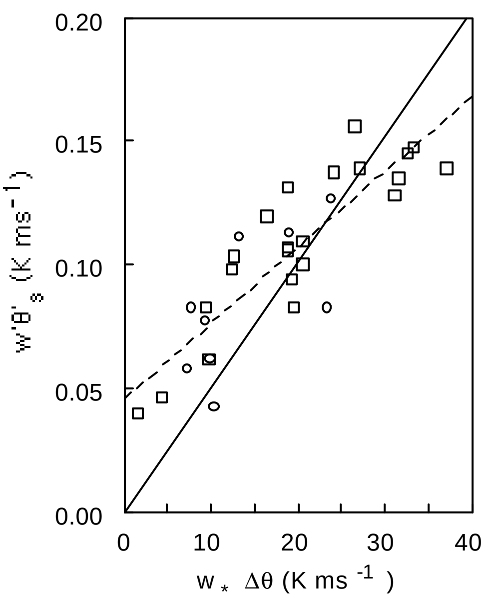

Fig. 6. Similar to Fig. 2, but for FIFE (circles) and Monsoon (squares).

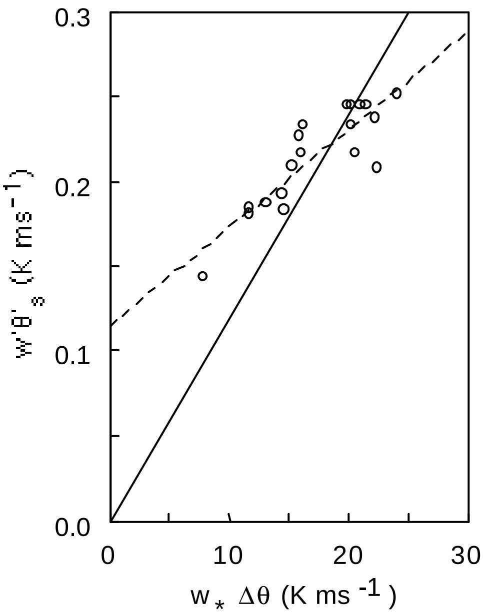

Fig. 7. Similar to Fig. 2, but for HAPER – MOBILHY.

Hignett (1998) noticed a similar characteristic. There is a tendency in those figures that the heat flux is non-zero when $w_* \cdot \Delta\bar{q}$ equals zero. The fact that so many diverse data sets exhibit the same characteristic suggests that there is some common physical process involved.

First, the BLX96 data were analyzed to test whether this non-zero intercept is related to an artifact of the Fourier filtering that was conducted before the flux calculation. Progressive bandwidth filters are applied to check if the trend is associated with fluxes contributed by the longer wavelengths. Band pass filter between a common short-wavelength cutoff of 0.02 km, and three different long-wavelength cutoffs: 1, 3, and 5 km were conducted, as shown in Fig 9. The mean variable ($\Delta\bar{q}$) is the same for these three filters, but the variables containing flux ($\overline{w'q'}_s$ and w_*) change. The data are clustered clearly for each related band pass filtering.

For this study, the regression lines are NOT forced to pass through the origin. The resulting flux intercepts at zero $\Delta\bar{q}$ are surprisingly uniform: 0.022 Kms^{-1}, 0.021 Kms^{-1} and 0.022 Kms^{-1} for the 5 km, 3 km and 1 km filters, respectively. This is a clue that the non-zero heat-flux intercept is not related to the size of the turbulent eddies, and is not an artifact of the filtering method.

However, the slopes (which determine C_{*H}) are different for the different filtering: C_{*H} = 0.0039 (± 0.0011), 0.0035 (± 0.0009), and 0.0026 (± 0.0010), respectively. The coefficients decrease as longer wavelengths are removed from the flux calculation, which suggests that there was no spectral gap between 1 and 5 km for this data set. The rms errors are 0.0078 Kms^{-1}, 0.0064 Kms^{-1} and 0.0066 Kms^{-1}, respectively. This means that the C_{*H} results (related to the line slope, not to the intercept) presented next for BLX96 must all be qualified as being associated with a wavelength range of 20 m to 5 km.

Compared to the results from the previous sections where the regression line was forced to pass through the origin, these new regressions explain much more of the variance. The unexplained variance is now reduced to about 50% of the previous value. Therefore, this nonzero intercept is significant, and is not related to the longer wavelengths that are retained in the flux calculation.

The regression procedure is repeated allowing non-zero intercepts for the other field sites. The plots of these results are shown in Figs. 2 – 7. The result for TOGA - COARE is not plotted in the figure, because the intercept is almost zero and the slope is practically the same as the previous value.

Best-fit lines with nonzero intercepts $\overline{w'q'}_o$ were found for the following linear regression equation:

$$\overline{w'q'}_s = C_{*H} \cdot w_* \cdot \Delta\bar{q} + \overline{w'q'}_o \qquad (6)$$

The BLX96 data from the three different sites are relatively clustered together, and coalesce into a single line. Therefore, the data are analyzed together, yielding a slope of C_{*H} = 0.0039 (± 0.0011) and an intercept of $\overline{w'q'}_o$ = 0.022 (± 0.008) Kms^{-1}. For BLX83, C_{*H} = 0.0032 (± 0.0017) with intercept $\overline{w'q'}_o$ = 0.040 (± 0.017) Kms^{-1}. For Koorin, C_{*H} = 0.0038 (± 0.0018) and $\overline{w'q'}_o$ = 0.064 (± 0.030) Kms^{-1}.

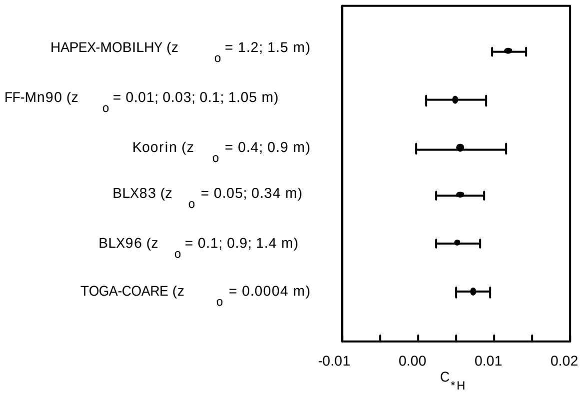

Fig. 8. Summary over all field experiments studied here of best fit values of mixed-layer transport coefficients for heat C_{*H}. Parenthetical values are reported aerodynamic roughness lengths z_o, which for most sites includes either a range of roughness estimates, or different sub domains with different roughnesses. The values in this figure assume that zero flux occurs with zero potential temperature difference, which is shown later to be a poor assumption. Error bars indicate plus/minus one standard deviation.

The FIFE and Monsoon 90 data are analyzed together as discussed before. The slope and intercept are C_{*H} = 0.0031 (± 0.0017) and $\overline{w'q'}_o$ = 0.045 (± 0.017) Kms^{-1}. For TOGA – COARE, C_{*H} = 0.0073 (± 0.0021), but the intercept is near zero [-0.00002 (± 0.0015) Kms^{-1}]. For HAPEX – MOBILHY, C_{*H} = 0.0058 (± 0.0009) and $\overline{w'q'}_o$ = 0.11 (± 0.014) Kms^{-1}. These results are summarized in Fig 10.

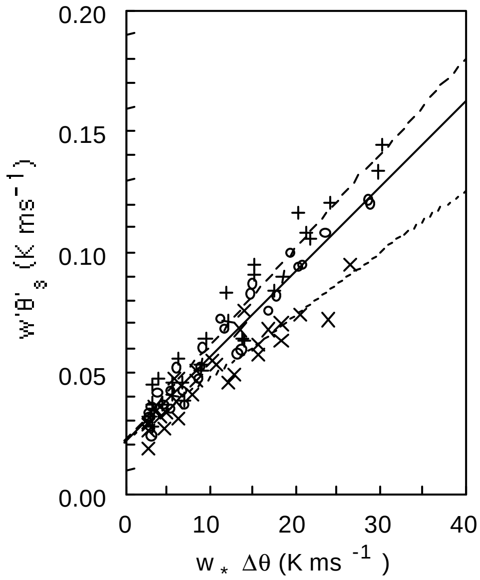

FIG. 9. BLX96 data progressively band pass filtered between 0.02 km and three different long-wavelength cutoffs: 5 km (pluses), 3 km (circles) and 1 km (crosses). The corresponding linear-regression lines are dashed, solid, and dotted.

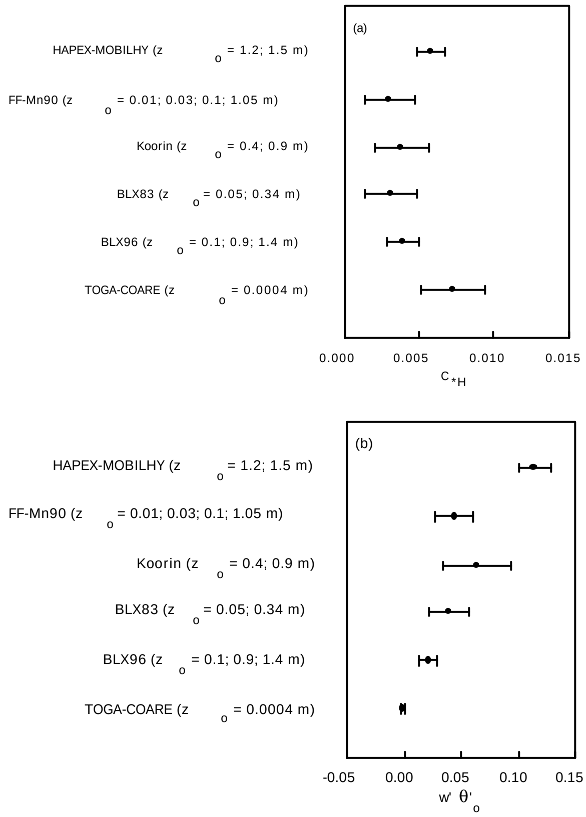

FIG. 10. Summary over all field experiments studied here of the best fit regression coefficients of (a) slope and (b) intercept for the heat flux equation $\overline{w'q'}_s = C_{*H} \cdot w_* \cdot \Delta\overline{q} + \overline{w'q'}_o$. Parenthetical values are the z_o values reported for each experiment. Error bars indicate plus/minus one standard deviation in both figures.

The BLX96 data exhibit less scatter compared to the others, probably because the measured variables (heat fluxes and surface skin potential temperatures) were more statistically robust because of the long flight legs of order 70 km. Also, determination of UL potential temperatures were likely more robust as well, because of the extensive vertical averaging over much of the UL, as described earlier.

The BLX83 fluxes, which were measured from much shorter legs (in average were about less than 1/3 times the BLX96 legs), lack the statistical robustness (Lenschow and Stankov, 1986) and thus exhibit more scatter. The high pass filtering for wavelengths less than 6.25 km (Stull, 1988) in the BLX83 flux calculations might also cause that data to deviate slightly from that of BLX96. For the FIFE and Monsoon 90 data, the scatter is probably due to measurements being made from different platforms.

Figs. 8 and 10a show significant overlap of C_{*H} values from BLX83, BLX96, FIFE and Monsoon 90. This is further supported in Fig. 10, where those data sets are plotted together. When the BLX83, BLX96, FIFE and Monsoon 90 data are analyzed together, the ML coefficient for heat flux is C_{*H} = 0.0035 (± 0.0015) and the intercept is $\overline{w'\theta'}_o$ = 0.34 (± 0.015) Kms^{-1}, as is shown by the solid line in Fig 11. When all the data sets are combined and weighted by their respective numbers of data points, the resulting regression coefficients are C_{*H} = 0.0046, and $\overline{w'\theta'}_o$ = 0.039 Kms^{-1}.

Based on the data in Fig. 10, it appears that the intercept values $\overline{w'\theta'}_o$ depend on the field site locations, with the smallest for the TOGA - COARE and the largest for HAPEX – MOBILHY. However, neither C_{*H} nor $\overline{w'\theta'}_o$ show any significant dependence on surface roughness z_o, so some other characteristic of these sites could be having an influence on the heat flux coefficients.

6. HYPOTHESES FOR NON-ZERO INTERCEPT

In attempting to explain this non-zero intercept, the intercept values are correlated with ML scaling variables, latitude, time of day (because of the possible influence of sun angle and view angle on remotely measured surface skin temperatures), and local land-use characteristics (such as albedo and vegetation cover). No significant correlations were found.

Two alternative hypotheses are suggested that could explain why there are positive fluxes when the surface skin has colder potential temperature than the mid-ML. One is an equilibrium situation of direct infrared (IR) radiative heat transfer from the surface to the bottom of the ML. The other is a non-equilibrium situation related to the time lag in response of surface-layer temperature during rapidly decreasing insolation such as occurs near sunset.

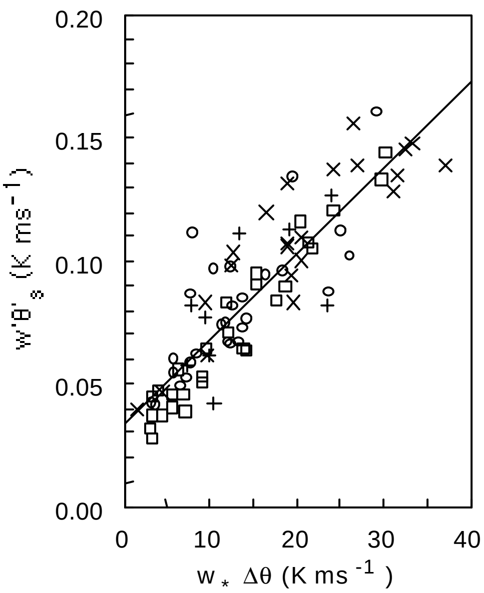

Fig. 11. Linear regression with non-zero heat-flux intercept for the combined data of BLX83 (circles), all three BLX96 sites (squares), FIFE (pluses), and Monsoon 90 data (crosses).

6.1. Hypothesis 1 – IR Radiative Transfer

There can be non-zero IR flux from the surface skin to the air, even when $\Delta\overline{\theta}$ is zero. This is possible because in adiabatic environments of $\Delta\overline{\theta}$ = 0, the corresponding $\Delta\overline{T} = \overline{T}_{skin} - \overline{T}_{UL}$ is still positive, and the Stefan-Boltzmann law states that emitted radiation depends on T, not on θ. Thus, there could be greater upward IR flux from the surface than downward flux from the air, causing net radiative convergence and heating in the bottom of the ML. This radiatively heated air is buoyant and creates convective thermals, the net result being that IR radiative flux is converted to a turbulent heat flux in the bottom of the ML. While analogous nighttime cooling due to direct radiative divergence in the bottom 5 m of the surface layer has been reported in the literature (e.g., Fuggle and Oke, 1976), we have been unable to find references for the afternoon heating situation of radiative convergence in the surface layer.

For this IR convergence process to successfully explain the observations, humidity must be sufficiently low so that the optical depth of the IR radiation is sufficiently large (i.e., the atmosphere must be sufficiently translucent to IR) that the air absolute temperature can be different from the ground IR temperature even for an adiabatic lapse rate. However, the humidity should not be too low, or else the radiative heating would be spread over such a thick portion of the ML that there would be no hot layers to generate thermals.

Pursuing this hypothesis further, one can speculate that over the ocean where surface-layer humidities are very high, the air is relatively opaque to most of the IR radiation from the sea surface. Hence, the altitude of absorption of the upward IR flux from the sea is so close to the surface that the air and the sea surface are virtually the same absolute temperature. With no absolute temperature difference, there would be no net IR flux, thereby causing no turbulent flux and hence zero intercept. This could explain why the TOGA-COARE intercept is near zero.

Over land, it would seem unlikely that there would be a step change in heat flux across ($w_* \cdot \Delta\overline{\theta}$) = 0. Extrapolating the lines in Fig 10 to the left (see Fig 12) suggests that there could be a

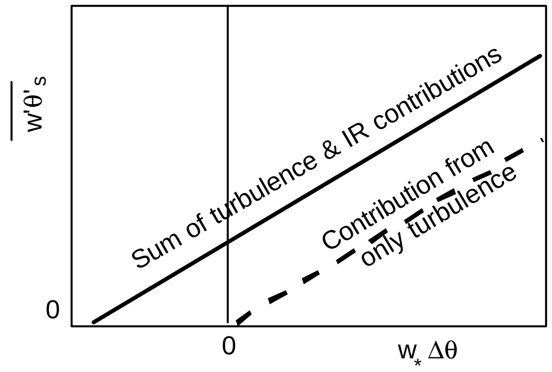

Fig. 12. Sketch of how positive values of near-surface heat flux could exist with zero and negative values of potential temperature difference. Based on Fig. 11 with additional speculation on the contribution from direct IR radiation convergence.

range of negative values of ($w_* \cdot \Delta\bar{q}$) where positive heat flux could occur. Namely, there could be an upward heat flux from a surface with colder potential temperature to a UL with warmer potential temperature. As this flux is opposite to the sign of the potential temperature difference, it is called a counter-difference flux, analogous to counter-gradient fluxes used in local (small-eddy) descriptions of turbulence. Such a counter-difference flux cannot be explained by a lack of nonlocal transport in the parameterization, because the UL-skin difference is already a nonlocal one.

Furthermore, it is unlikely that the counter-difference flux is caused by entrainment from the free atmosphere, because that would cause a negative heat flux as warm air (in a potential temperature sense) is entrained downward. So again, IR radiative convergence from the surface is left as a plausible explanation. Such IR heating, if it exists, would likely occur for all cases of positive surface heat flux, not just for flux values near zero or negative.

Such IR divergence might also help explain why field observations of surface energy budgets do not balance very well (Foken and Onkley, 1995). This problem with an unbalanced surface budget might occur if net radiation is measured at a different height in the surface layer than turbulent sensible heat flux, and would be related to the accuracy of the assumption that fluxes are constant with height in the surface layer. Also, the IR flux might contribute to the failure of energy-balance Bowen-ratio (EBBR) methods of estimating surface fluxes at sunrise and sunset (Stull, 1988).

6.2. Hypothesis 2 – Surface Layer Time Lag

Static instabilities in the atmosphere are not eliminated instantly. It takes roughly a convective time scale (order of 15 minutes) to remove most of the hot air from the surface layer by mixing it upward. The existence of a super adiabatic lapse rate in the surface layer is evidence of this finite response time. Namely, if mixing had been faster, the static instability associated with air heated by the underlying surface would have created such rapid upward mixing that the surface layer lapse rate would be well mixed with the rest of the ML, leaving a nearly adiabatic temperature profile in the surface layer.

Nieuwstadt and Brost (1986) presented a related evidence, where decaying but nonzero

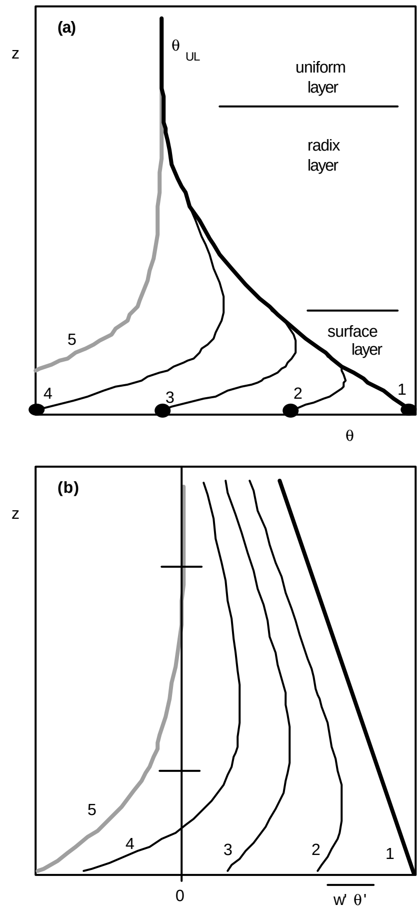

Fig. 13. Sketch of the evolution of profiles of (a) potential temperature; and (b) kinematic heat flux during the evening transition from surface heating to cooling. The heavy solid line represents the initial stationary situation in midafternoon, and the heavy dashed line represents the final stationary situation in late evening. The thin lines represent nonequilibrium evolution from the initial to final states. For state 3, zero potential temperature difference between the surface and uniform layer would be accompanied by positive heat flux at the base of the uniform layer due to nonlocal movement of thermals from the relative maximum of potential temperature. This situation could explain the non-zero intercept of Fig. 11. Even at state 4, a positive heat flux could occur near the base of the uniform layer even though the surface skin is colder than the uniform layer, and even though the turbulent heat flux has become negative right at the surface. This situation would correspond to counter-difference fluxes.

convective circulations were observed after the surface became cooler than the ML in the evening. Suppose that this decaying process happens as sketched in Fig 13a, with fluxes evolving as shown in Fig 13b. Namely, as the surface skin cools, it cools the very bottom of the ML by conduction. However, higher in the surface layer is a layer of warmer air remaining from tens of minutes earlier that has not had sufficient time to be completely eliminated by convection. The heat flux measured at the top of the surface layer would thus be caused by convection from this disappearing warm layer.

Other evidence for such a process is found in non-equilibrium simulations of boundary-layer evolution and turbulence, such as transilient turbulence theory (T3). T3 reacts to static instabilities by creating mixing that acts over finite time intervals (Stull, 1993). In the paper by Driedonks and Stull (1987, see time 1600 GMT in their Fig. 10c), during the late afternoon when surface heat flux was decreasing rapidly in a T3 model of the boundary layer, there was a temporary condition of greater positive heat flux near the top of the surface layer than at the surface. For such a case, the heat flux at the top of the surface layer would be greater than expected from the potential temperature difference between the surface skin and the ML. Such a situation would lead to a heat-flux vs. temperature difference curve similar to that plotted in Fig. 11 here rather than from the cooler surface skin.

6.3. Recommendation

The arguments of the previous two subsections are just speculation. The field program pursued other research avenues, and was unable to perform the follow-up work needed to test these two hypotheses. To investigate the first hypothesis, future boundary layer experiments should consider measuring the vertical profile of IR radiation vertical convergence over perhaps a wider range of wavelengths than is traditionally obtained.

The second hypothesis is more difficult to test, because one needs ensemble, line, or area averages of turbulent fluxes simultaneously at different heights, but one cannot use Taylor's hypothesis to substitute time averages at points for the ensemble average because of the nonstationarity. Perhaps large-eddy simulation can be used to help investigate this issue. Also, we have presented this hypothesis for nonzero (positive) heat flux intercept for afternoon situations when insolation is decreasing. However, near solar noon when the insolation is approximately steady, this argument would suggest that the heat flux intercept would be zero. In morning when insolation is increasing, the heat-flux intercept would be negative according to this hypothesis.

7. CONCLUSIONS

New data from the BLX96 field experiment were analyzed, and old data from BLX83, Koorin, TOGA-COARE, HAPEX-MOBILHY, FIFE, and Monsoon 90 were re-analyzed to test surface heat flux parameterization. In summary the followings were found:

1) For heat flux, C_{*H} does not show evidence of being correlated with z_o.

2) There is non-zero heat-flux intercept $\overline{w'\theta'_o}$ in 6 of the 7 data sets, implying that there can be a turbulent heat flux even when $\Delta\overline{\theta}$ = 0. When all the data sets are combined and weighted by their respective numbers of data points, the regression of the equation $\overline{w'\theta'}_s = C_{*H} \cdot w_* \cdot \Delta\overline{\theta} + \overline{w'\theta'}_o$ yields the following empirical values for the regression coefficients: C_{*H} = 0.0046, and $\overline{w'\theta'_o}$ = 0.039 Kms^{-1}. Factors that cause the intercept value to vary from experiment to experiment have yet to be identified, but do not appear to be correlated with z_o.

3) It is inferred that the non-zero intercept is a special case of a more general scenario of positive heat flux that can exist for slightly negative values of $\Delta\overline{\theta}$, as plotted in Fig 12a. This is a counter-difference flux, and two alternative hypotheses are suggested to explain it.

One is direct radiative heating caused by convergence of IR radiation from the ground. This happens because $\Delta\overline{T}$ can be positive even though $\Delta\overline{\theta}$ is negative, within a limited range. This IR radiative effect could explain why measured surface energy budgets often do not quite balance, and why the energy-balance Bowen-ratio method of estimating fluxes gives unreliable oscillations of flux near sunrise and sunset.

The other is a nonequilibrium situation in late afternoon and early evening, when rapidly decreasing insolation causes a decreasing surface skin temperature. Warmer air near the top of the surface layer created earlier would still be mixing away, causing a greater positive heat flux than could be explained by the instantaneous value of $\Delta\overline{\theta}$

4) To test these hypotheses, it is recommended that future boundary layer field campaigns include measurement of the vertical profile of IR flux convergence during the daytime, and that methods such as remote sensing be used to give line or area averaged turbulent fluxes at a variety of heights during the nonstationary situation of rapidly decaying turbulence near sunset.

REFERENCES

Andre, J. C., J. P. Goutorbe and A. Perrier, 1986: HAPEX - MOBILHY: A hydrologic atmospheric experiment for the study of water budget and evaporation flux at the climate scale. *Bull. Amer. Meteor. Soc.*, **67**, 138 - 144.

Beljaars, A. C. M., 1995: The parameterization of surface fluxes in large scale models under free convection. *Quart. J. Roy. Meteor. Soc.*, **121**, 255 - 270.

Berg, L. K., R. B. Stull, E. Santoso, J. P. Hacker, 1997: *Boundary Layer Experiment - 1996 (BLX96) Airborne Scientist Flight Log*. Boundary Layer Research Team Technical Note BLRT- 97-1. 116 pp.

Bond, G. and D. Alexander, 1994: *TOGA COARE Meteorology Atlas*. TOGA - COARE International Project Office. 336 pp

Brutsaert, W., A. Y. Hsu and T. J. Schmuggle, 1993: Parameterization of surface heat fluxes above a forest with satellite thermal sensing and boundary-layer soundings. *J. Appl. Meteor.*, **32**, 909 - 917.

Brutsaert, W. and M. Sugita, 1992: Regional surface fluxes from satellite-derived surface temperature (AVHRR) and radiosonde profiles. *Bound.-Layer Meteor.*, **58**, 355 - 366.

Chang, H.-R. and R.L. Grossman, 1998: Evaluation of bulk surface flux algorithms for light wind conditions using data from the Coupled Atmosphere-Ocean Response Experiment (COARE). *Quart. J. Roy. Meteor. Soc.* (in press).

Clarke, R. H. and R. R. Brook, 1979: *The Koorin Expedition, Atmospheric Boundary Layer Data over Tropical Savannah Land*. Bureau of Meteorology, Australian Government Publishing Service, Canberra. ISBN-0-642-01484-1. 359 pp.

Crum, T. D., R. B. Stull and E. W. Eloranta, 1987: Coincident lidar and aircraft observations of entrainment into thermals and mixed layers. *J. Climate Appl. Meteor.* **26**, 774 - 788.

Foken, T. and S. Oncley, 1995: Meeting summary: Workshop on instrumental and methodical problems of land surface flux measurements. *Bull. Amer. Meteor. Soc.*, **76**, 1191-1193.

Fuggle, R.F. and T.R. Oke, 1976: Long-wave radiative flux divergence and nocturnal cooling of the urban atmosphere. *Boundary-Layer Meteor.*, **10**, 113-120.

Grant, A. L. M. and P. Hignett, 1998: Aircraft observations of the surface energy balance in TOGA - COARE. *Quart. J. Roy. Meteor. Soc.*, **124**, 101 - 122.

Greischar, L. and R. B. Stull, 1998: Convective transport theory for surface fluxes, tested over the western Pacific warm pool. *J. Atmos. Sci*. (in press).

Holton, J.R., 1992: *An Introduction to Dynamic Meteorology (3rd Ed.).* Academic Press. 511 pp.

Kustas, W. P. et al., 1991: An interdisciplinary field study of the energy and water fluxes in the atmosphere - biosphere system over semiarid rangelands: Description and some preliminary results. *Bull. Amer. Meteor. Soc.*, **72**, 1683 - 1706.

Kustas, W. P., L. E. Hipps and K. S. Humes, 1995: Calculation of basin-scale surface fluxes by combining remotely-sensed data and atmospheric properties in a semiarid landscape *Bound.-Layer Meteor.*, **73**, 105 - 124.

Kustas, W. P., T. J. Schmugge and L. E. Hipps, 1996: On using mixed-layer transport parameterizations with radiometric surface skin temperature for computing regional scale sensible heat flux. *Bound.-Layer Meteor.*, **80**, 205 - 221.

LeMone, M. A., S. Oncley, T. Horst., R. L. Grossman, J. K. Lundquist, R. McMillen, B. Hicks, R. Coulter, and G. Klazura, 1998: CASES-97: Diurnal variation of the fair-weather PBL. *Proceedings, Special Session on Hydrology*, Amer. Meteor. Soc., 88 -92.

LeMone, M.A., and R.L. Grossman, 1998: Evolution of potential temperature and moisture during the morning: CASES-97. *Preprints, 13th Symposium. on Boundary Layers and Turbulence, Dallas, Texas. January 1999*. Amer. Meteor. Soc.

Lenschow, D. H. and B. B. Stankov, 1986: Length scale in the convective boundary layer. *J. Atmos. Sci.*, **43**, 1198 - 1209.

Lundquist, J.K., 1997: *A Test of Convective Transport Theory*. Comprehensive Exam Thesis, Program in Atmospheric and Oceanic Science, Univ. of Colorado - Boulder. 32 pp.

Lundquist, J.K., 1998: Testing Convective Transport Theory with CASES 97 data. Submitted to *J. Applied Meteor*.

Mahrt, L. and M. Ek, 1993: Spatial variability of turbulent fluxes and roughness lengths in HAPEX-MOBILHY. *Bound.-Layer Meteor.*, **65**, 381 - 400.

Nieuwstadt, F.T.M. and R.A. Brost, 1986: The decay of convective turbulence. *J. Atmos. Sci.*, **43**, 532-546.

Perry, E. M. and M. S. Moran, 1994: An evaluation of atmospheric corrections of radiometric surface temperatures for a semiarid rangeland watershed. *Water Resour. Res.*, **30**, 1261 -1269.

Press, W. H., B. P. Flannery, S. A. Teukolsky and W. T. Vetterling, 1992: *Numerical Recipes in FORTRAN: The Art of Scientific Computing*, Second Ed., Cambridge University Press 963 pp.

Santoso, E, 1999: *Surface Fluxes and Vertical*

Profiles in the Radix layer. PhD Dissertation, University of British Columbia, 184pp.

Santoso, E., 2000: Parameterization of surface momentum flux during convective conditions. *J. Sains & Tekn. Mod. Cuaca*, **1**, 33 – 44.

Santoso, E. and R. B. Stull, 1998: Wind and temperature profiles in the radix layer, the bottom fifth of the convective boundary layer. *J. Appl. Meteor.*, **37**, 545 - 558.

Santoso, E. and R.B. Stull, 1999: Use of synthetic data to test flight patterns for a boundary-layer field experiment. *J. Atmos. and Ocean Tech.*, **16,** (in press).

Sellers, P. J., F. G. Hall, G. Asrar, D. E. Strebel and R. E. Murphy, 1988: The first ISLSCP field experiment (FIFE). *Bull. Amer. Meteor. Soc.*, **69**, 22 - 27.

Smedman-Hogstrom, A. S. and U. Hogstrom, 1978: A practical method for determining wind frequency distributions for the lowest 200 m from routine meteorological data. *J. Appl. Meteor.*, **17**, 942 - 954.

Sorbjan, Z., 1995: Toward evaluation of heat fluxes in the convective boundary layer. *J. Appl. Meteor.*, **34**, 1092-1098.

Sorbjan, Z., 1997: Comments on “A convective transport theory for surface fluxes.” *J. Atmos. Sci*., **54**, 576-578.

Stewart, J. B., W.P. Kustas, K.S. Humes, W.D. Nichols, M.S. Moran, and H.A.R. DeBruin, 1994: Sensible heat flux-radiometric surface temperature for eight semiarid areas. *J. Appl. Meteor.*, **33**, 1110 - 1117.

Stull, R. B., 1988: *An Introduction to Boundary Layer Meteorology*. Kluwer Academic Publishers, Dordrecht, The Netherlands. 666 pp.

Stull, R.B., 1993: Review of nonlocal mixing in turbulent atmospheres: transilient turbulence theory. *Boundary-Layer Meteor.*, **62**, 21-96.

Stull, R. B., 1994: A convective transport theory for surface fluxes. *J. Atmos. Sci*., **51**, 3 - 22.

Stull, R. B., 1995: *Meteorology Today for Scientists and Engineers*. Wadsworth (West) ITP, Belmont, California. 385 pp.

Stull, R. B., 1997a: Reply (to comments on “A convective transport theory for surface fluxes). *J. Atmos. Sci*., **54**, 579.

Stull, R. B., 1997b: Convective transport theory and the radix layer. *NATO Advanced Study Institute Buoyant Convection in Geophysical Flows*. Pforzheim, Germany.

Stull, R.B. and E.W. Eloranta, 1984: Boundary Layer experiment - 1983. *Bull. Amer. Meteor. Soc.*, **65**, 450 - 456.

Stull, R.B. and E.W. Eloranta, 1985: A case study of the accuracy of routine, fair-weather cloud-base reports. *National Weather Digest*, **10**, 19-24.

Stull, R. B., E. Santoso, L. Berg and J. Hacker, 1997: Boundary layer experiment - 1996 (BLX96). *Bull. Amer. Meteor. Soc.*, **78**, 1149-1158.

Sun, J. et al., 1996 : Scale dependence of air-sea fluxes over the western equatorial Pacific. *J. Atmos. Sci.*, **53**, 2997 - 3012.

Wieringa, J., 1980: Representativeness of wind observations at airports. *Bull. Amer. Meteor. Soc.*, **61**, 962 - 971.

Wieringa, J., 1986: Roughness-dependent geographical interpolation of surface wind speed averages. *Quart. J. Roy. Meteor. Soc.*, **112**, 867 - 889.

DATA PENULIS

EDI SANTOSO, lahir di Jakarta, 12 Maret 1960. Menyelesaikan S1 di Jurusan Geofisika & Meteorologi, ITB (1985). Menyelesaikan S2 bidang Atmospheric Sciences, di University of Wisconsin – Madison, USA (1993). Menyelesaikan S3 bidang Atmospheric Science, di University of British Columbia, Vancouver, Canada (1999). Bekerja di UPT Hujan Buatan BPP Teknologi sejak 1986. Sebagai Research Assistant di University of Wisconsin – Madison (1994 – 1995) dan di University of British Columbia (1996 – 1999). Sebagai Teaching Assistant di University of British Columbia (1998 – 1999).